

Supplementary Material

Cucurbiturils regulating Fe₃O₄-Au nanoparticles as a multi-function platform for Cd²⁺ sensing and nitrocompound catalysis

Zhaorui Song,^a Chenrui Jiang,^a Meriem Fizir,^b Fangqi Wang,^a Sijing Ye,^a Pierre Dramou,^{a,*} Hua He^{a, c, d,*}

^a Department of Analytical Chemistry, China Pharmaceutical University, Nanjing, 211100, China

^b Laboratoire de Valorisation des Substances Naturelles, Université Djilali Bounaâma, Khemis-Miliana, Algérie.

^c Key Laboratory of Biomedical Functional Materials, China Pharmaceutical University, Nanjing 211100, China

^d Key Laboratory of Drug Quality Control and Pharmacovigilance, Ministry of Education, China Pharmaceutical University, Nanjing 211198, China

* Corresponding author.

Tel: +86 025 86185008; Fax: +86 025 86185008.

E-mail addresses: jcb_321@163.com; dochehua@163.com.

Experimental section

Chemical and Materials Ferric chloride ($\text{FeCl}_3 \cdot 6\text{H}_2\text{O}$), Ferrous chloride ($\text{FeCl}_2 \cdot 4\text{H}_2\text{O}$), Chloroauric acid ($\text{HAuCl}_4 \cdot 4\text{H}_2\text{O}$), NaBH_4 , NaOH were purchased from Sinopharm Chemical Reagent Co., Ltd (China). Cadmium chloride (CdCl_2), 4-nitrophenol (4-NP) were acquired from Macklin Biochemical Co., Ltd (Shanghai, China). L-cysteine (L-cys) and Metronidazole were obtained from Sigma-Aldrich (Shanghai, China). Cyclohexanocucurbit[6]uril ($\text{CB}^*[6]$) and cucurbit[7]uril ($\text{CB}[7]$) were purchased from Shanghai Nafu Biotechnology Co., Ltd (Shanghai, China). All solutions were prepared with distilled water. All chemicals in this work were of analytical grade and used without further purification.

Characterization X-Ray diffraction patterns were recorded using a D/MAX-2500PC X-ray diffractometer (Rigaku Corporation) with $\text{Cu-K}\alpha$ ($\lambda = 1.5406 \text{ \AA}$) radiation and operated at a generator voltage and an emission current of 40 kV and 35 mA. Scan range (2θ) was recorded from 10° to 80° and scan speed was set at $10^\circ \text{ minute}^{-1}$. Transmission electron microscopy (TEM) images were obtained on a JEOL JEM 2100F microscope operated at 120 kV operated at an accelerating voltage of 120 kV. Magnetisation measurements was carried out using vibrating sample magnetometer (JC08 HH-15, Bei Xin Ke Yuan Instrument Co., Ltd) under a varying magnetic field from -10000 to 10000 Oe at 300K. Scanning electron microscope (SEM) image and elemental analysis were performed by scanning electron microscope (SEM) equipped with energy-dispersive X-rays (EDX) at 200 kV accelerating voltage (EDAX TEAMTM). Particle size was measured with Zetasizer Nano ZS90 (Malvern Instruments, UK). Cd^{2+} concentrations were determined using ICP-OES (ICPE-9000, Shimadzu, Japan). UV-vis absorption spectra were acquired with a UV-vis spectrophotometer (UV-1800, Shimadzu, Japan) at room temperature. Infrared (IR) measurements were obtained with a Nicolet Magna 550 spectrometer (Thermo Scientific). The pH was measured with a PHS-3C pH meter (REX, Shanghai, China). Furthermore, molecular modeling calculations are optimized at the B3LYP/6-31G(d) level of density functional theory using the Gaussian 03 program.

Synthesis of $\text{Fe}_3\text{O}_4\text{-Au@CB}[n]$

This novel multifunctional platform is constructed by three steps, which are the preparation of L-cys functionalized Fe_3O_4 NPs,¹ in-situ reduction of HAuCl_4 and the surface modification of CBs. Due to $\text{Fe}_3\text{O}_4\text{-cys}$ NPs has abundant functional groups, HAuCl_4 can be absorbed on the surface of $\text{Fe}_3\text{O}_4\text{-cys}$ NPs, and then reduct in-situ by NaBH_4 and get $\text{Fe}_3\text{O}_4\text{-Au}$ NPs (Acting as **catalyst I**). The outer of $\text{Fe}_3\text{O}_4\text{-Au}$ NPs with positive charges can bind with the carbonyl-lined portals of CBs by electrostatic adsorption and then finally obtain $\text{Fe}_3\text{O}_4\text{-Au@CB}^*[6]$ (Acting as **probe I and catalyst II**, respectively) and $\text{Fe}_3\text{O}_4\text{-Au@CB}[7]$ (Acting as **probe II and catalyst III**, respectively).

Synthesis of $\text{Fe}_3\text{O}_4\text{-cys}$ NPs and AuNPs: Fe_3O_4 NPs were prepared by co-precipitation method.¹ For synthesis of L-cys functionalized Fe_3O_4 NPs ($\text{Fe}_3\text{O}_4\text{-cys}$ NPs), 250 mg Fe_3O_4

NPs were pretreated with 100 mL HCl solution (1M) under ultrasound for 30 min. Then these Fe₃O₄ NPs were collected using an external magnet and washed 5 times and then resuspended with 100 mL water. 70 mL L-cys aqueous solution (10 mg mL⁻¹) was added into 100 mL Fe₃O₄ NPs above with ultrasonic treatment for 30 min and then stirred for 3 h at 60 °C. Subsequently, the synthesized Fe₃O₄-cys NPs were magnetically separated and washed completely with water, and then resuspended with 100 mL water. As for AuNPs, they were obtained by the reduction reaction of HAuCl₄ (10 mg mL⁻¹) in the presence of NaBH₄ (0.1 M) in ice-bath.

Preparation of Fe₃O₄-Au@CB[n] : Fe₃O₄-Au NPs were firstly synthesized. Briefly, 600 μL HAuCl₄ (10 mg mL⁻¹) was dispersed in 98 mL water and then mechanically stirred for 10 min at ice bath. Meanwhile, 100 μL Fe₃O₄-cys NPs was dispersed in 1.9 mL water with ultrasound for 10 min. A volume of 0.5 mL ice-cold, freshly prepared 0.1 M NaBH₄ was added and then the solution turned wine red immediately. 2 mL Fe₃O₄-cys solution was added dropwise and stirred continuously for 2 h at ice bath and then obtained Fe₃O₄-Au NPs solution.

The preparation of Fe₃O₄-Au@CB*[6] solution was as follows : 1 mL 2 mg mL⁻¹ CB*[6] was added into the fresh prepared Fe₃O₄-Au NPs aqueous solution dropwise and the mechanically stirred for 2 h at room temperature. The product was separated magnetically and washed with water for 3 times, and resuspended in 25 mL distilled water.

The preparation of Fe₃O₄-Au@CB[7] solution was as follows: 1 mL 2 mg mL⁻¹ CB[7] was added into the new prepared Fe₃O₄-Au NPs aqueous solution and the rest of the process was similar to that of probe I. Ultimately, this solution was dried and a brown magnetic powder was obtained.

Developed probe I for the sensitive detection of Cd²⁺.

A certain volume of probe I solution was mixed with a series of different concentrations of Cd²⁺ solution and the mixtures were mechanically oscillated for 30 min at room temperature, and then UV-vis spectra was recorded. The effect of various parameters like reaction time, pH, probe volume and ion inference were investigated and then a linear relationship between the concentrations of Cd²⁺ and the absorbance changes of probe I was expected to be established.

For further practical application, water samples collected from Ming lake (China pharmaceutical university, CPU) with the addition of different concentrations of Cd²⁺, which were used as the simulated samples. After centrifugation at 11000 rpm for 10 min, water samples were filtered through 0.22 μm millipore filter for experimental use. Simulated samples were mixed with probe I for 30 min, and then UV-vis spectra was measured. Meanwhile, the formed nanocomposite precipitation was removed rapidly by a permanent magnet. The fortified concentration and supernatant concentrations of Cd²⁺ were detected by ICP-OES.

Developed heterogeneous catalysts for the catalytic reduction of nitrocompounds

The reduction of 4-nitrophenol (4-NP) with NaBH₄ as the reductant was usually selected as a model reaction. It was used to investigate the catalytic performance of three catalysts. A typical experiment was implemented as follows: 20 μL 4-NP (10 mM), 20 μL catalyst I (1 mg mL⁻¹) and 2.8 mL distilled water were added into a cuvette. This solution was treated with ultrasound for 20 s and then 0.2 mL NaBH₄ (0.1 M) was introduced into the mixture with gentle shaking. The color of solution changed from yellow to transparent as the reaction proceeded and the reaction process was monitored by UV-vis spectrum. Meanwhile, Fe₃O₄-Au@CB*[6] NPs and Fe₃O₄-Au NPs were also used to be investigated and then compare the differences of catalytic properties. Furthermore, the reusability of these catalysts were also explored under the same conditions above. These catalysts were magnetically separated at the end of each cycle and then washed with distilled water for next time.

The catalytic mechanism of three catalysts were investigated thoroughly. Specifically, the selective catalytic reduction (SCR) of catalyst III to a series of structural analogs of 4-NP including the nitro, carboxyl, amidogen, hydroxyl, aldehyde and carbonyl groups, were also investigated in the same conditions above.

Results and Discussion

FT-IR: FT-IR spectra of Fe₃O₄ (a), Fe₃O₄-cys (b) and Fe₃O₄-Au NPs (c) show that all of them have a characteristic of Fe-O absorption peak at 588 cm⁻¹ due to its symmetric stretching vibration (Fig. S1). Fe₃O₄-cys NPs exhibit the characteristic absorption bands of L-cys. 2372 cm⁻¹ assigns to the S-H stretching vibration. The sharp peak of Fe₃O₄-Au NPs at 2372 cm⁻¹ disappears, implying the formation of Au-S bond. The sharp peak at 1487 cm⁻¹ disappears, due to electrostatic adsorption between protonated amine (-NH₂) and surface-bound AuCl⁴⁻/AuCl²⁻ ions.¹⁶

XRD: The XRD patterns of Fe₃O₄ NPs and Fe₃O₄-Au NPs show that Fe₃O₄-Au NPs display diffraction peaks at $2\theta = 38.31^\circ, 44.56^\circ, 64.78^\circ$ and 77.62° , which are assigned to the (111), (200), (220) and (311) planes of gold with a cubic phase (JCPDS card no. 04-0784) (Fig. S2). The absence of Fe₃O₄ NP diffraction peaks in the XRD pattern of Fe₃O₄-Au NPs indicates that the surface of the Fe₃O₄ NPs has been effectively covered with a layer of AuNPs. Meanwhile, the chemical composition of Fe₃O₄-AuNPs was provided by energy dispersive X-ray (EDX) spectroscopy. From Fig. S3, it is clear that these core-shell NPs contain Fe, O and Au elements, and the inset table exhibits the content of the three elements, which distinctly confirms the coexistence of Fe, Au and O. Elemental mapping images reveal that both Fe and O elements with high-density are distributed at the center, and the Au

element is homogeneously distributed, confirming the presence of Au on the surface of Fe₃O₄ NPs.

VSM: The hysteresis loops of Fe₃O₄ NPs and Fe₃O₄-Au NPs are shown in Fig. S6. Fe₃O₄-Au NPs have no remanence or coercivity, and the saturation magnetization is 35.6 emu g⁻¹, which confirms their good superparamagnetism. Meanwhile, compared with the saturation magnetisation of uncoated Fe₃O₄ NPs (62.2 emu g⁻¹), the decrease of Fe₃O₄-Au NPs offers strong evidence that an efficient layer of AuNPs is located outside the magnetic core. The inset pattern also demonstrates the convenient separation of Fe₃O₄-Au NPs by an external magnet.

Selective catalytic reduction (SCR): From Table S4, we can find that carboxyl, amidogen and hydroxyl groups cannot be reduced by NaBH₄ and catalytic reduction was also not observed even under the combined action of NaBH₄ and catalyst III. The nitro group cannot be reduced by NaBH₄. However, it can be reduced by NaBH₄ and catalyst III together and the conversion rate can reach up to 97%. The aldehyde group can only be reduced by NaBH₄ or by NaBH₄ and catalyst III together, and all the conversion rates are above 95%. However, the reduction time is the same and the rate constant k values are close to each other, which can be explained by the fact that the aldehyde group can be easily reduced by the strong reductant due to its high reactivity. The carbonyl group can be reduced by NaBH₄ alone and also catalyzed by catalyst III and NaBH₄ together. The reduction reaction can be quickened to some extent with the addition of catalyst III, and the conversion rate is higher than 97%. In conclusion, aldehyde and carbonyl groups can be easily reduced by NaBH₄, and only nitro groups can be selectively and efficiently reduced under the action of catalyst III.

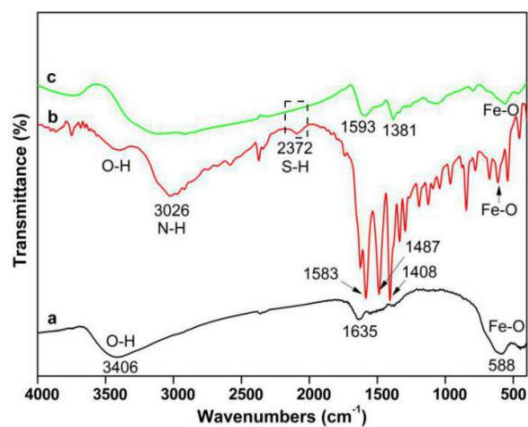


Fig. S1. FT-IR spectra of Fe_3O_4 (a), Fe_3O_4 -cys (b) and Fe_3O_4 -Au NPs (c).

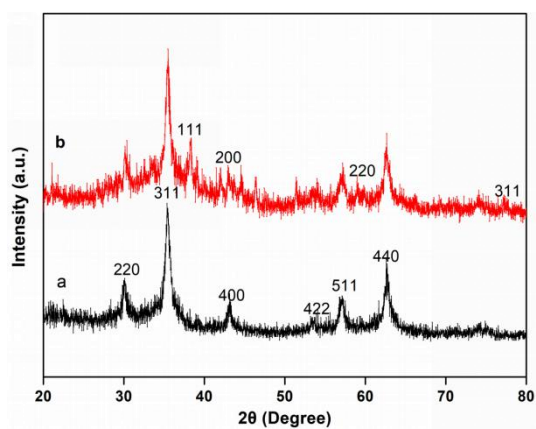


Fig. S2. XRD patterns of Fe_3O_4 NPs (a) and Fe_3O_4 -Au NPs (b).

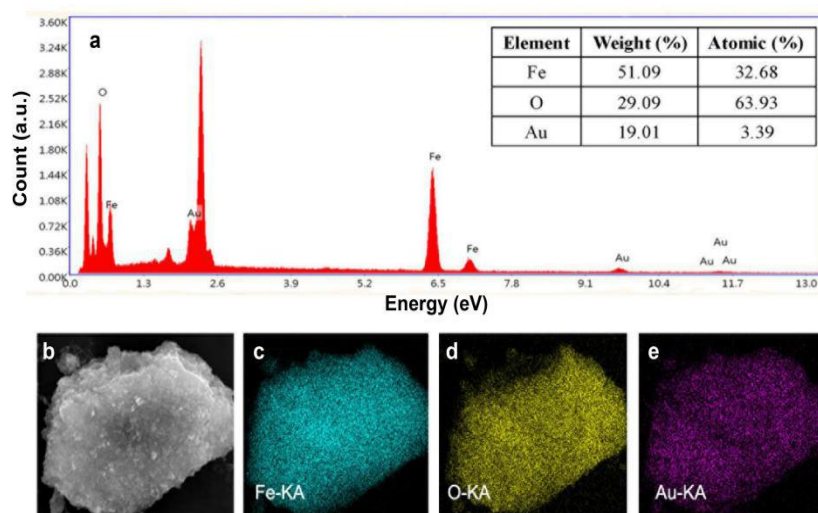


Fig. S3. EDX spectra of Fe_3O_4 -Au NPs (a); STEM image of Fe_3O_4 -Au NPs (b); EDX elemental mapping images (c-e) of Fe_3O_4 -Au NPs.

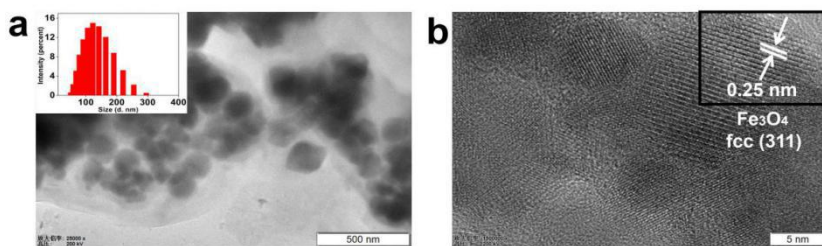


Fig. S4. a) TEM and b) HRTEM images of Fe_3O_4 NPs.

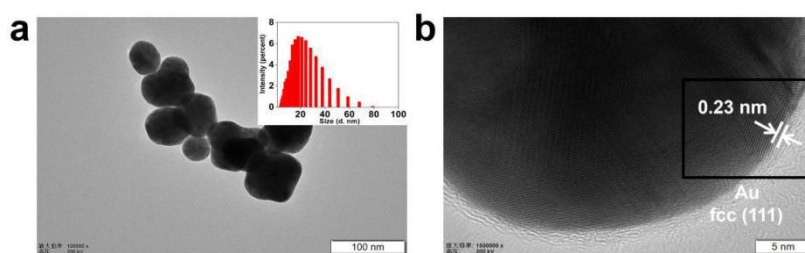


Fig. S5. a) TEM and b) HRTEM images of Au NPs.

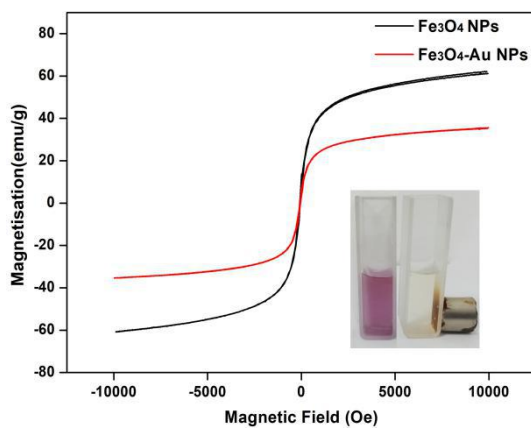


Fig. S6. The magnetic hysteresis loops of Fe_3O_4 NPs (black) and Fe_3O_4 -Au NPs (red).

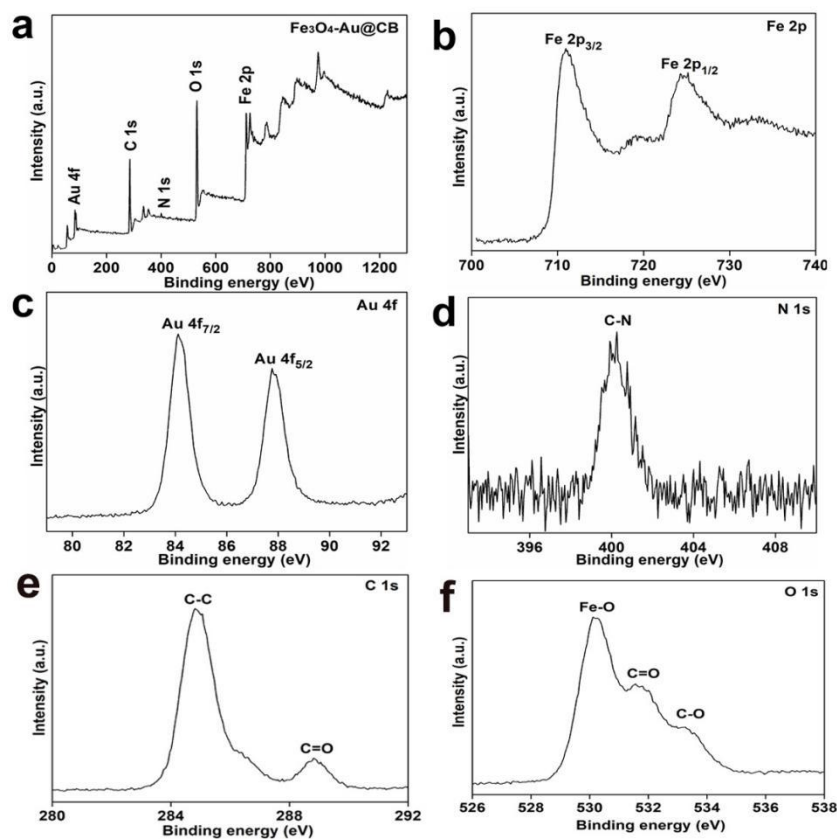


Fig. S7. XPS spectra of the as-prepared $\text{Fe}_3\text{O}_4\text{-Au@CB}$ (CB*[6] and CB[7]). a) XPS survey spectra. b) Fe 2p spectrum of the $\text{Fe}_3\text{O}_4\text{-Au@CB}$. c) Au 4f spectrum of the $\text{Fe}_3\text{O}_4\text{-Au@CB}$. d-f) the N 1s, C 1s and O 1s spectrum of $\text{Fe}_3\text{O}_4\text{-Au@CB}$.

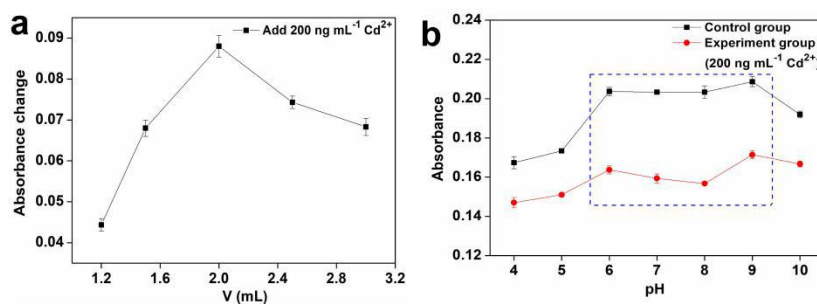


Fig. S8. a) The effect of probe I volume on the detection ($n=3$); b) The effect of different pH on the detection ($n=3$).

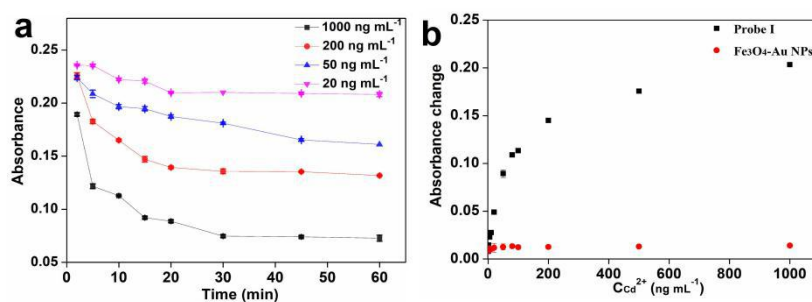


Fig. S9. a) Plot of absorbance at 545 nm versus time with the addition of different concentrations of Cd^{2+} ($n=3$). b) The absorbance change of probe I and $\text{Fe}_3\text{O}_4\text{-Au}$ NPs with the addition of different concentrations of Cd^{2+} ($n=3$).

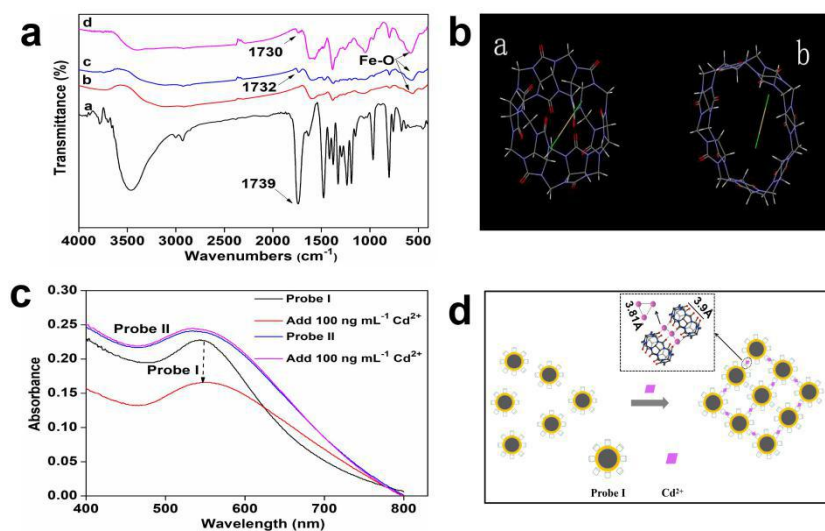
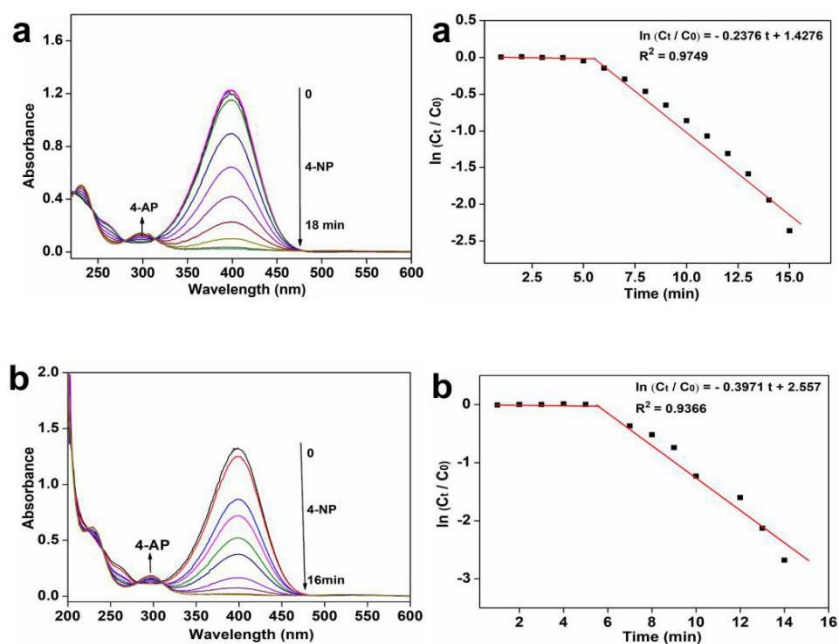


Fig. S10. a) FT-IR spectra comparison of $\text{CB}^*[6]$ (a), $\text{Fe}_3\text{O}_4\text{-Au}$ NPs (b), probe I (c) and the complex of Cd^{2+} binding with probe I (d). b) Molecular modeling of the energy-minimized structure of $\text{CB}^*[6]\text{-Cd}^{2+}$ complex (a) and $\text{CB}^*[7]\text{-Cd}^{2+}$ complex (b). c) UV-vis absorption spectra changes of probe I and probe II by adding $100 \text{ ng mL}^{-1} \text{ Cd}^{2+}$, respectively. d) Schematic diagram describe the detection principle of Cd^{2+} inducing the aggregation of probe I.



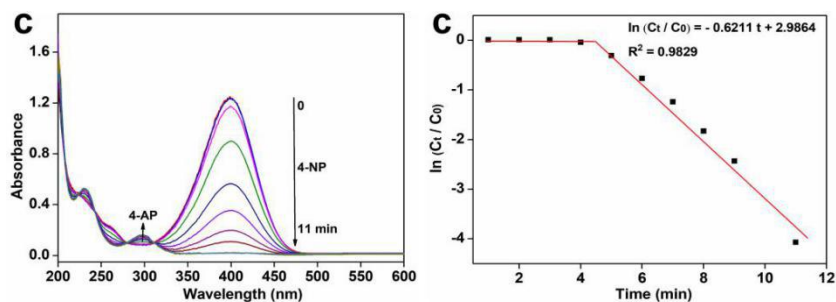


Fig. S11. Time - dependent UV- vis spectral changes (left) and the linear relationship of $\ln(C_t/C_0)$ as a function of time (right) for 4-NP catalyzed by catalyst I (a), II (b) and III (c).

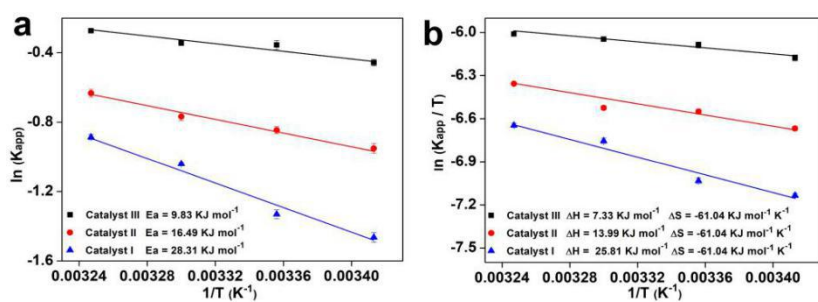


Fig. S12. a) Plots of $\ln k$ (a) and b) $\ln(k/T)$ versus $1/T$ for the reduction reaction of 4-NP with three catalysts.

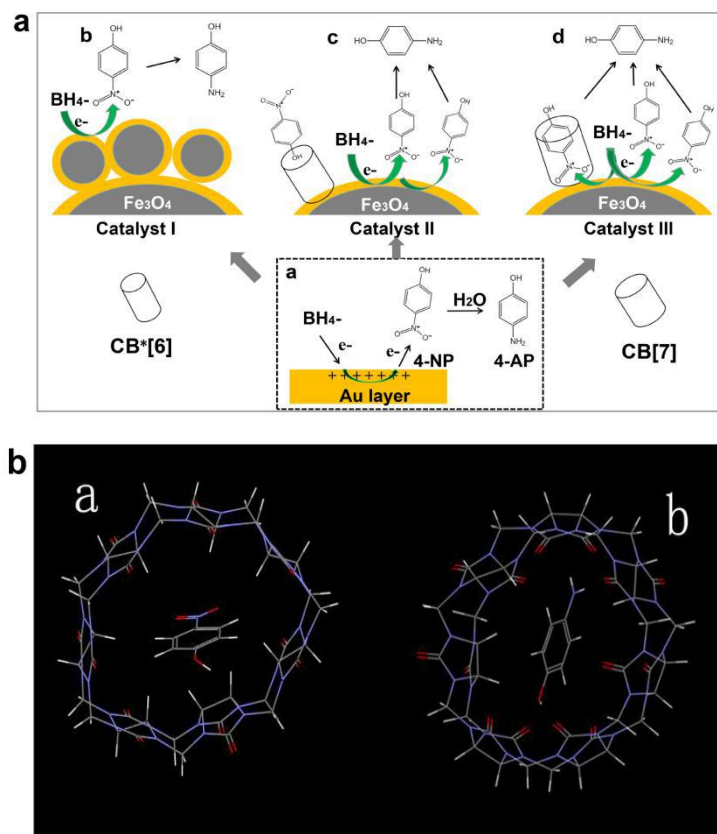


Fig. S13. a) Schematic diagram describing catalytic reduction of 4-NP by three catalysts. b) Molecular modeling of the energy-minimized structure of CB[7]-4-NP complex (a) and CB[7]-4-AP complex (b).

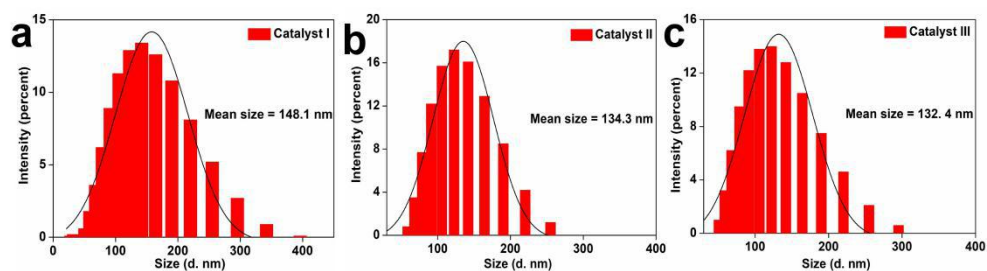


Fig. S14. The size distribution of catalyst I (a), catalyst II (b) and catalyst III (c).

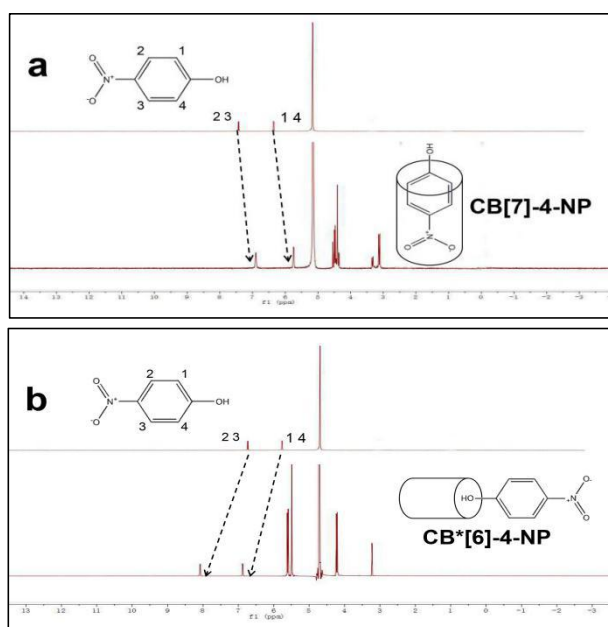


Fig. S15. a) ^1H NMR (600 MHz) spectra of CB[7]-4-NP complex and b) CB*[6]-4-NP complex.

Table S1 Determination of Cd^{2+} in simulation samples using the proposed method.

Methods	Added (ng mL^{-1})	Detected ^[a] (ng mL^{-1})	Recovery (%)	CV (%)	<i>p</i>
This method	5	5 ± 0.4	106.1	7.5	> 0.05
	30	30 ± 3.2	101.5	10.4	
	70	70 ± 3.6	99.3	1.1	
ICP-OES	5	5 ± 0.2	99.5	3.1	> 0.05
	30	30 ± 0.7	100.4	2.3	
	70	70 ± 1.1	100.3	1.6	

[a] Value = mean \pm SD (n=3)

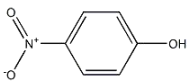
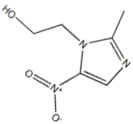
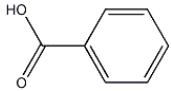
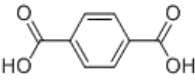
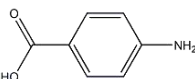
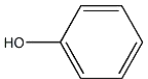
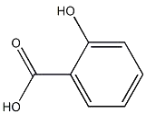
Table S2 The kinetic rate constant k of two catalysts with five consecutive cycles.

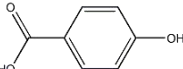
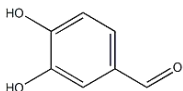
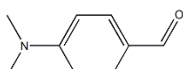
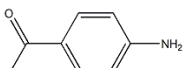
Cycle number	1	2	3	4	5
$k_{\text{catalyst III}}$	0.62 min^{-1}	0.36 min^{-1}	0.21 min^{-1}	0.10 min^{-1}	0.08 min^{-1}
$k_{\text{catalyst I}}$	0.24 min^{-1}	0.22 min^{-1}	0.09 min^{-1}	0.05 min^{-1}	0.01 min^{-1}

Table S3 Summary of Fe_3O_4 -Au catalysts for reduction of 4-NP.

Catalyst	Amount (mg)	k_{app} (min^{-1})	Reduction time (min)	Recycle number	Ref.
Catalyst III	0.05	0.62	11	5	This work
Au- Fe_3O_4	2	0.63	10	6	21
heterostructures					
Fe_3O_4 @Au NPs	10	-	68	6	22
Au- Fe_3O_4 NPs	2	0.38-0.63	10	-	23
Fe_3O_4 @ SiO_2 @Au@mSiO ₂	3	0.2-0.42	12	7	24
rGO- Fe_3O_4 -Au	4	0.686	5	8	25

Table S4 Selective catalytic reduction (SCR) of catalyst III to different functional groups.

Groups	Chemical Name	Structure	Time (min)	k_{app} ^[a] (min^{-1})	C ^[b] (%)	Addition
Nitro	p-Nitrophenol (4-NP)		7	0.621	98.46	1 ^[c]
			—	—	—	2 ^[d]
Carboxyl	Metronidazole		10	0.482	97.05	1
			—	—	—	2
	Benzoic acid		—	—	—	1
			—	—	—	2
Amidogen	Terephthalic acid (TPA)		—	—	—	1
			—	—	—	2
	Para aminobenzoic acid (PABA)		—	—	—	1
Hydroxyl			—	—	—	2
	Phenol		—	—	—	1
			—	—	—	2
	Salicylic acid		—	—	—	1
			—	—	—	2

Aldehyde	p-hydroxybenzoic acid (PHBA)		—	—	—	1
			—	—	—	2
	Protocatechualdehyde		9	0.503	98.12	1
				9	0.511	97.54
	4-Dimethylamino benzaldehyde		4	0.817	95.83	1
				4	0.809	96.88
Carbonyl	4-Aminoacetophenone		30	0.119	98.83	1
			40	0.102	97.49	2

[a] The values of apparent kinetic rate constant. [b] Conversion rate. [c] Adding NaBH₄ and catalyst I. [d] Only adding NaBH₄.

[1] S. Banerjee, N. P. Kumar, A. Srinivas, S. Roy, *J. Hazard. Mater.*, 2019, **375**, 216-223.